

¹ Binocular combination in the autonomic nervous system

² Federico G. Segala^{1*}, Aurelio Bruno^{1,2}, Joel T. Martin^{1,3},
Anisa Y. Morsi¹, Alex R. Wade^{1,4} & Daniel H. Baker^{1,4}

³ ¹Department of Psychology, University of York, Heslington, York, YO10 5DD, United Kingdom.

⁴ ²School of Psychology and Vision Sciences, University of Leicester, Leicester, LE1 7RH, United Kingdom.

⁵ ³School of Philosophy, Psychology and Language Sciences, University of Edinburgh, Edinburgh, EH8 9AD,
⁶ United Kingdom.

⁷ ⁴York Biomedical Research Institute, University of York, Heslington, York, YO10 5NG, United Kingdom.

⁸ *Corresponding author

⁹ E-mail:federico.segala@york.ac.uk (FGS)

¹⁰ **1 Abstract**

¹¹ Pupil diameters are regulated by the autonomic nervous system, which combines light signals across the eyes
¹² independently of the visual cortex. Distinct classes of retinal photoreceptor are involved in this process, with
¹³ cones and rods driving the initial constriction and intrinsically photosensitive retinal ganglion cells main-
¹⁴ taining diameter over prolonged time periods. We investigated binocular combination by targeting different
¹⁵ photoreceptor pathways using a novel binocular multiprimary system to modulate the input spectra via silent
¹⁶ substitution. At the first harmonic of the modulation frequency, luminance and S-cone responses showed
¹⁷ strong binocular facilitation, and weak interocular suppression. Melanopsin responses were invariant to the
¹⁸ number of eyes stimulated. Notably, the L-M pathway involved binocular inhibition, whereby responses to
¹⁹ binocular stimulation were weaker than for monocular stimulation. The second harmonic involved strong
²⁰ interocular suppression in all pathways, but with some evidence of binocular facilitation. Our results are
²¹ consistent with a computational model of binocular signal combination (implemented in a Bayesian hier-
²² archical framework), in which the weight of interocular suppression differs across pathways. We also find
²³ pathway differences in response phase, consistent with different lag times for phototransduction. This work
²⁴ demonstrates for the first time the algorithm governing binocular combination in the autonomic nervous
²⁵ system.

²⁶ **2 Author Summary**

²⁷ Our pupils constantly adjust in size to control how much light enters the eye: in brighter conditions the
²⁸ pupils will reduce in size, and in dimmer conditions they will increase in size. This process, known as the
²⁹ pupillary light response, is usually taken for granted but is crucial for vision, and is controlled automatically
³⁰ by the body's nervous system. Different types of light-sensing cells in the retina, the photoreceptor cells,
³¹ contribute to this response: some respond quickly to changes in light, while others maintain responses over
³² longer periods. In our study, we explored how signals from the two eyes are combined to regulate pupil size.
³³ Using a new type of visual stimulation that allowed us to selectively target specific classes of photoreceptor
³⁴ cells, we found that the way the two eyes' signals are combined depends on which class of photoreceptor cells
³⁵ is involved. For example, some photoreceptor classes showed cooperation between the eyes, while others
³⁶ showed competition. By revealing these distinct patterns of signal combination, our work provides new
³⁷ insight into how light information is integrated in the pupils.

³⁸ 3 Introduction

³⁹ The autonomic nervous system regulates many involuntary bodily processes, including the constriction and
⁴⁰ dilation of the pupils in response to light [1]. The anatomical pathway from the retina to the subcortical
⁴¹ nuclei controlling the pupillary light response (PLR) is well established: it includes the Pretectal Olivary
⁴² nucleus (PON), the Superior Cervical ganglion and the Edinger-Westphal nucleus, which project to the iris
⁴³ sphincter muscles that directly control the pupil size [1]. Evidence of a binocular component to the PLR is
⁴⁴ shown by the consensual response of the pupil (stimulation of one eye will cause constriction of the other
⁴⁵ eye) [2]. The anatomical segregation of the subcortical pathway from the rest of the brain means that this
⁴⁶ binocular combination of signals must occur independently of the cortical processes of binocular integration
⁴⁷ required for visual perception. Our recent work [3] has shown that the algorithm underlying binocular
⁴⁸ combination of light in the pupil pathway differs from that in the cortex. Here we extend this paradigm to
⁴⁹ compare binocular combination in different photoreceptor pathways that feed into the autonomic nervous
⁵⁰ system.

⁵¹ Different classes of retinal photoreceptors, including cones, rods and melanopsin-containing intrinsically
⁵² photosensitive retinal ganglion cells (ipRGCs), are directly involved in controlling and maintaining the size
⁵³ of the pupils [4–8]. Cones drive the initial rapid constriction of the pupils [9], while the slower and longer
⁵⁴ activation of the ipRGCs maintains constriction over a prolonged period of time and regulates the post-
⁵⁵ illumination pupillary response [4,10]. The ipRGCs are a recently discovered photoreceptor class [11] that
⁵⁶ express the photopigment melanopsin, and are involved in the regulation of the circadian rhythm [12,13],
⁵⁷ forming a major input to the PON [14]. The first direct evidence of the involvement of the ipRGCs in the
⁵⁸ PLR was shown in melanopsin knockout rats [15], resulting in the loss of the intrinsic photosensitivity of
⁵⁹ the cells and a reduced pupil constriction. Similar behaviour was later observed in primates and humans
⁶⁰ [16] using silent substitution (see Methods), where it was demonstrated that the PLR continues during light
⁶¹ presentation even when cone and rod signalling is blocked, indicating the primary role of the ipRGCs in
⁶² maintaining pupil constriction over a prolonged time.

⁶³ Binocular combination has been extensively studied in visual perception, where it is mediated by neurons in
⁶⁴ primary visual cortex [17]. For pattern vision, binocular summation occurs at threshold, such that a lower
⁶⁵ contrast is required to detect a target shown to both eyes than a target shown to one eye [18,19]. At higher
⁶⁶ contrasts, the phenomenon of ‘ocularity invariance’ is observed, in which the response to monocularly- and
⁶⁷ binocularly-presented patterns is equal [20,21]. This is explained by a process of interocular suppression
⁶⁸ that cancels out the additional excitatory drive caused by stimulating two eyes. Our recent work [3] showed

69 that cortical signal combination for luminance flicker is substantially more linear than for spatial patterns,
70 whereas there is evidence of interocular suppression in the pupil pathway. Here we measure the amplitude
71 of pupil modulations in response to flickering stimuli presented as light flux, or directed towards the L-M
72 cone, S-cone, and melanopsin pathways (see Figure 1e-l). Our key comparisons are between monocular and
73 binocular stimulation, and in a dichoptic masking condition where the two eyes are stimulated at different
74 frequencies. The results are interpreted using a contemporary model of binocular vision [22] implemented
75 within a hierarchical Bayesian framework.

76 4 Results

77 Figure 1m-p shows averaged waveforms of pupil diameter in response to binocular stimulation. For light
78 flux stimuli (Figure 1m) a strong modulation is apparent at the stimulation frequency (0.5Hz), which is also
79 clear in the Fourier amplitude spectrum (Figure 1q). For binocular stimulation of the L-M pathway, S-cone
80 pathway and melanopsin pathway, pupil modulations were less than 10% of the amplitude of the light flux
81 modulation (note the change in y-axis scale for the Fourier spectra), but still apparent at 0.5Hz in the Fourier
82 spectra (Figure 1n-p). We also observed a second harmonic response (at 1Hz) for all conditions, which was
83 weaker than the first harmonic for light flux and melanopsin stimulation, but stronger for L-M and S-cone
84 stimulation. The second harmonic is also apparent in the pupil waveforms shown in Figure 1n-p. Our main
85 analysis therefore focuses on the amplitude of the pupil modulations at both the first and second harmonic
86 frequencies across different stimulus conditions.

87 Figure 2a-d shows contrast response functions across stimulation conditions for responses at the first harmonic
88 of the main stimulation frequency (0.5Hz). In each plot, the response to monocular stimulation is given by
89 the red circles and typically increases monotonically as a function of stimulus (temporal) contrast. Relative
90 to monocular stimulation, binocular stimulation led to higher response amplitudes, indicating a binocular
91 facilitation effect, for the light flux and S-cone conditions (Figure 2a,c), and to some extent for the melanopsin
92 condition (Figure 2d). However, the L-M cone condition (Figure 2b) produced a binocular suppression effect,
93 where the response to binocular stimulation was weaker than the response to monocular stimulation (blue
94 squares below red circles). These results indicate that the magnitude of binocular facilitation differs across
95 photoreceptor pathway, suggesting heterogeneity in the underlying neural computation.

96 In contemporary models of binocular signal combination, the amount of binocular facilitation is determined
97 by the magnitude of interocular suppression, with strong suppression reducing facilitation [23]. We can
98 estimate the strength of interocular suppression by measuring how much monocular responses are reduced

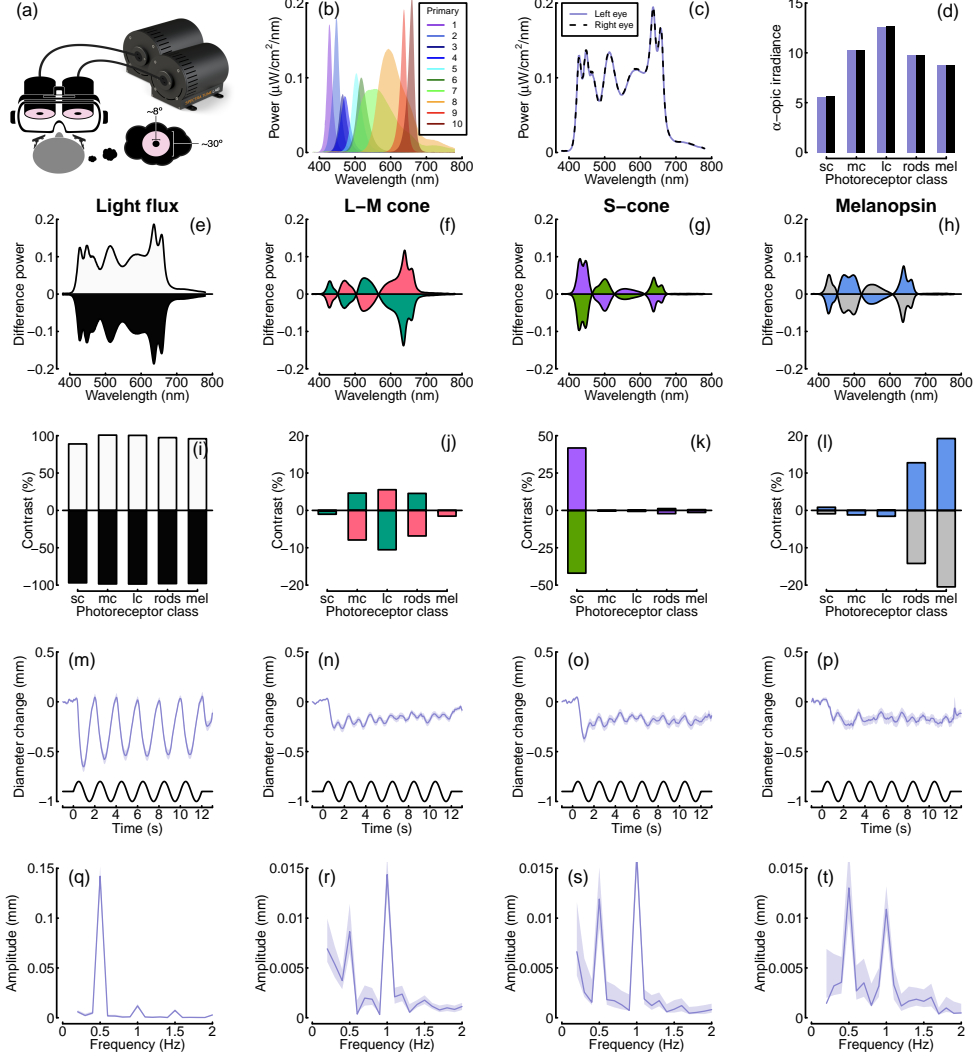


Figure 1: Summary of the spectral power distributions and alpha-optic irradiances for the background and each condition, as well as averaged pupil diameters and Fourier spectra. Panel (a) shows a schematic of the binocular stimulation system for presenting spectrally tuned modulations independently to each eye. The VR headset was attached to a clamp stand that the experimenters could use to adjust the height and align the headset with the eyes of the participant. The participant's head was supported by a chin rest to keep it in position throughout the experiment. Panel (b) shows the outputs of each LED primary at maximum intensity, and panels (c) and (d) show the overall spectral power distributions and the alpha-optic irradiances of the background spectra used for both eyes. The subsequent rows show the power differences (e-h), and photoreceptor contrasts (i-l) relative to the background, averaged pupil diameter waveforms (m-p) and Fourier spectra (q-t) for binocular stimulation. Column headings indicate the pathway stimulated, and shaded regions in panels m-t indicate bootstrapped 95% confidence intervals.

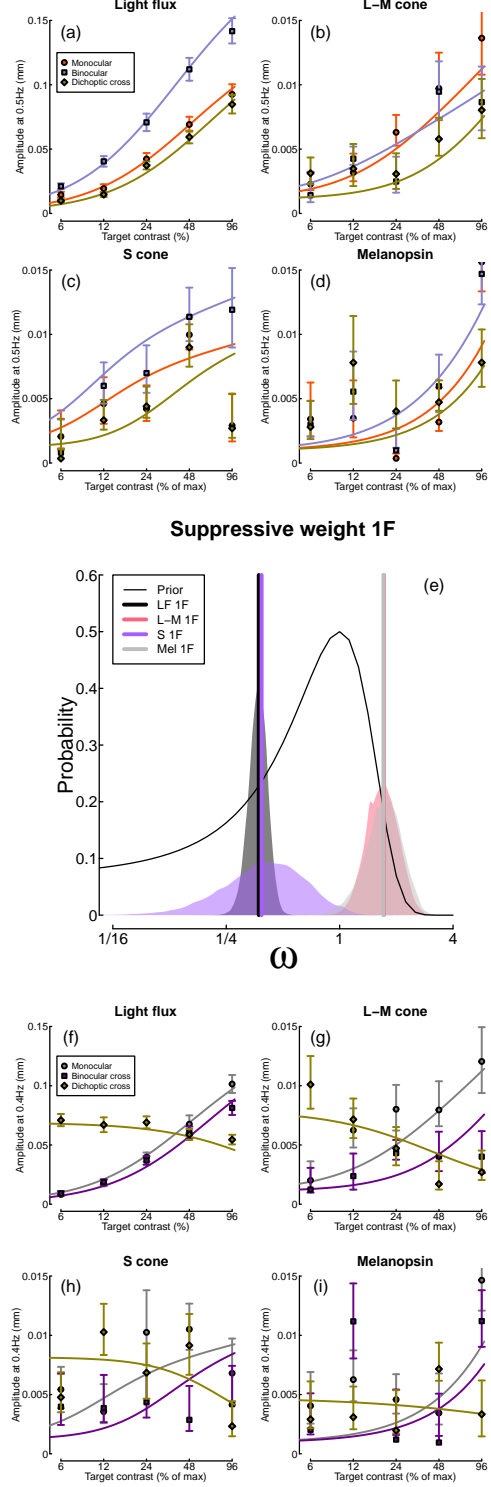


Figure 2: Contrast response functions for pupil modulations in response to flicker at 0.5Hz (panels a-d), and 0.4Hz (panels f-i), and posterior parameter distributions for the weight of interocular suppression (panel e). Within each panel (except panel e), data points are the coherently averaged amplitudes for each condition, and error bars indicate bootstrapped 95% confidence intervals. Curves show model fits using the maximum a posteriori (MAP) parameter values (see Table 1). In panel (e), vertical lines show the MAP estimates, and the thin black curve indicates the prior (note the logarithmic x-axis).

99 when a dichoptic ‘mask’ is shown to the other eye. In our paradigm, the two components flickered at
 100 different frequencies (0.5 and 0.4Hz) so that their responses remained distinct in the Fourier spectrum [24].
 101 The yellow diamond symbols in Figure 2a-d show the target responses in this condition, and in most cases
 102 were weaker than the monocular responses (red circles). The strongest dichoptic masking is found in the
 103 L-M condition, where we also observed the binocular suppression effect. Suppression can also be estimated
 104 from the responses at 0.4Hz (Figure 2f-i). The reduced amplitude in the binocular cross condition (where the
 105 two eyes received different temporal frequencies; purple squares) relative to the 0.4Hz monocular condition
 106 (grey circles), and the progressive decline in amplitude of the dichoptic cross response (yellow diamonds)
 107 also differ across photoreceptor conditions, showing similar differences to those observed at 0.5Hz.

108 To estimate the extent of interocular suppression for each photoreceptor pathway, we fitted each data set
 109 using a Bayesian hierarchical implementation of a simple binocular combination model [3,22]. Our primary
 110 objective was to compare posterior distributions of the weight of interocular suppression, which are shown in
 111 Figure 2e. Consistent with our earlier observations, the strongest suppressive weight corresponds to the L-M
 112 and Melanopsin conditions, and the weakest suppression corresponds to the light flux and S-cone conditions,
 113 with virtually no overlap between the posterior distributions for weak and strong suppression. The model
 114 fits were of good quality, as shown by the curves in Figure 2a-d,f-i. The fitted model parameters are given
 115 in Table 1.

Table 1: Summary of maximum a posteriori (MAP) parameter estimates for each data set.

Experiment	Z	k	w	p	q	Rmax
Light flux 1F	95.77	0.00083	0.37	1.32	1.24	0.0905
L-M cone 1F	49.82	0.00109	1.71	1.50	1.21	0.0032
S cone 1F	63.00	0.00121	0.39	1.94	1.79	0.0042
Melanopsin 1F	79.61	0.00094	1.71	1.29	0.76	0.0025
Light flux 2F	48.81	0.00089	1.24	1.15	0.88	0.0039
L-M cone 2F	66.00	0.00075	0.95	1.10	0.82	0.0050
S cone 2F	75.94	0.00097	2.22	1.41	0.83	0.0018
Melanopsin 2F	67.94	0.00101	1.37	0.90	0.49	0.0035

116 At the second harmonic frequencies, the levels of suppression were more uniform across different photore-
 117 ceptor pathways (see Figure 3). In general, suppression estimates were near or above 1 (see lower rows of
 118 Table 1), with substantial overlap between the posterior distributions (Figure 3e). The contrast response

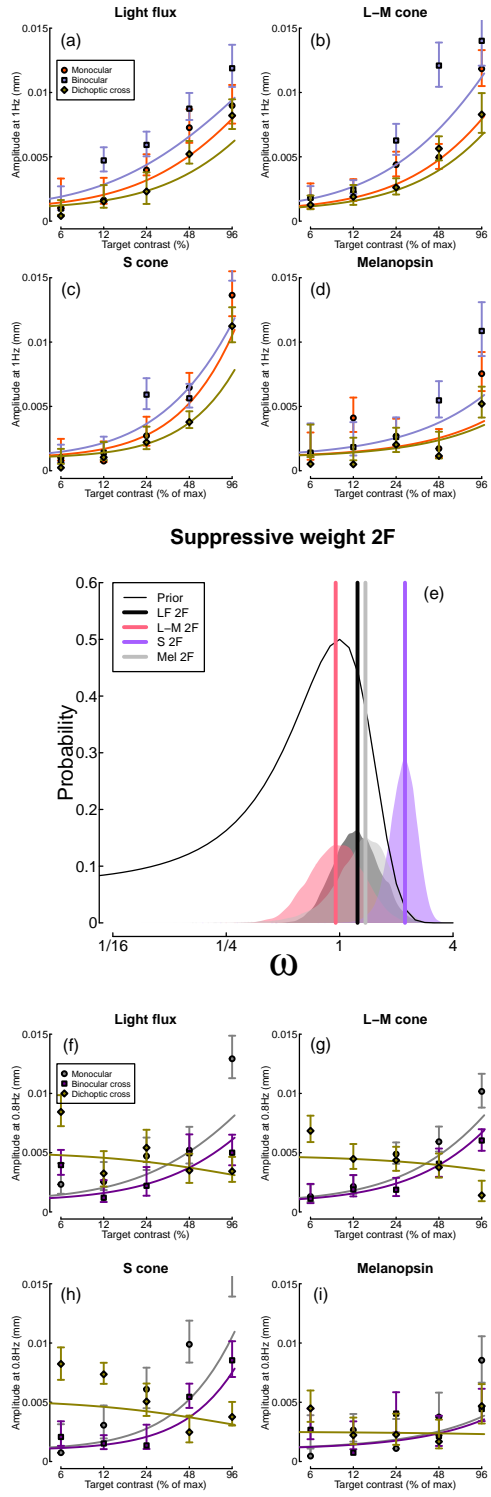


Figure 3: Responses at the second harmonic frequencies (1Hz and 0.8Hz), in the same format as Figure 2.

119 functions also looked more uniform, and generally involved less binocular facilitation and more interocular
 120 suppression than were seen at the first harmonics. The L-M condition now featured the weakest suppressive
 121 weight, and the strongest binocular facilitation, which was the opposite pattern seen at the first harmonic.

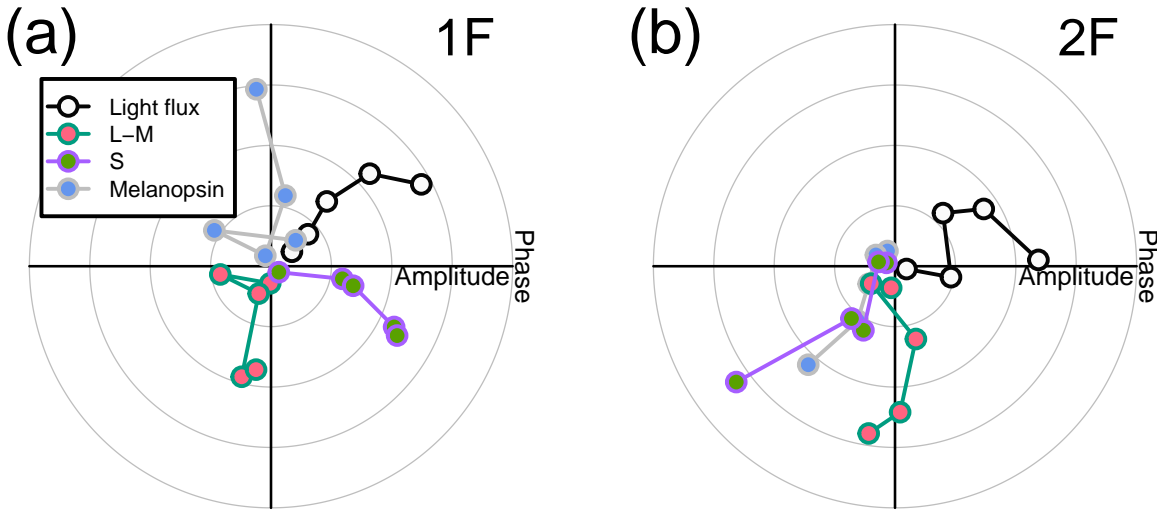


Figure 4: Pupil phase plots at the first and second harmonic frequencies for the light flux, melanopsin, L-M pathway and the S-cone pathway conditions. Panel (a) shows the pupil response at the first harmonic frequency during binocular stimulation. Panel (b) shows the pupil response at the second harmonic frequency during binocular stimulation. The five data points for each pathway correspond to the five contrast levels displayed. In panel (a) the light flux amplitudes have been scaled down by a factor of 10 to enable comparison with the other conditions.

122 Finally, we inspected the response phase of our four stimulation conditions, given previous reports that
 123 these differ across pathways [7], and may be in antiphase for melanopsin and S-cone signals. Figure 4 shows
 124 the phase angles for the first (a) and second (b) harmonic frequencies for binocular stimulation (monocular
 125 stimulation produced very similar results). At the first harmonic, melanopsin and S-cone signals differed in
 126 phase by more than 90 degrees, though they were not fully in antiphase. The light flux and L-M responses
 127 were approximately in antiphase to each other, however this is likely due to our choice to modulate L+M- in
 128 the first half-cycle of the sine wave (corresponding to a luminance increase in the light flux condition), and
 129 L-M+ in the second half-cycle (corresponding to a luminance decrease in the light flux condition). Had we
 130 reversed this phase arrangement, we would likely have seen a close phase correspondence between the L-M
 131 and light flux conditions (another way to think about this is that L-cone decreases and M-cone increases
 132 are processed like luminance increases). Phase differences between the light flux, S-cone and melanopsin
 133 conditions are likely attributable to different lags in phototransduction at the earliest stage (i.e. in the
 134 retina). At the second harmonic frequency (Figure 4b), the light flux condition was again out of phase with

135 the other three, and was approximately in quadrature phase with the L-M condition, and in antiphase with
136 both the S-cone and melanopsin conditions (which were in phase with each other). We note that the marked
137 phase differences between conditions make the possibility that our results are dominated by rod activity
138 relatively unlikely (e.g. in the L-M and melanopsin conditions, which have very different phase profiles).

139 5 Discussion

140 We used binocular pupillometry and silent substitution to measure monocular and binocular responses of
141 the pupils to flickering stimuli when stimulating specific photoreceptor pathways. In all four experiments, we
142 were able to record contrast response functions at both the first and the second harmonic frequencies. All
143 experiments showed that binocular combination in the autonomic nervous system happens in a non-linear
144 manner, with evidence of different magnitudes of interocular suppression depending on the photoreceptor
145 pathway. This pattern of results was confirmed by a computational model, which allowed us to compare the
146 weight of interocular suppression for each pathway. We found that at the first harmonic frequency the L-M
147 and melanopsin pathways involved strong suppression, whereas the light flux and S-cone pathways involved
148 weaker suppression. Suppression was strong in all four pathways at the second harmonic frequency. Finally,
149 the phase of the pupil response revealed different lag times for the different pathways at the first and second
150 harmonic frequencies.

151 This is the first study to investigate binocular interactions in the melanopsin pathway directly. A previous
152 meta-analysis [25] indicated that there may be a substantial binocular facilitation effect in the circadian
153 pathway, as indexed by melatonin suppression (melatonin is a hormone released by the pineal gland; its
154 production is suppressed by exposure to bright light, particularly when the melanopsin-containing ipRGCs
155 are stimulated). In brief, monocular stimulation of the ipRGCs requires up to ten times the signal strength
156 to produce an equivalent effect to binocular stimulation. This superadditive effect implies an absence of
157 interocular suppression, and perhaps the presence of either a highly compressive nonlinearity, or an AND-style
158 neural operation. Our findings here are very different - we do not see substantial binocular facilitation effects
159 in response to melanopsin modulation, and our data indicate that interocular suppression is very strong.
160 Moreover, by measuring the full contrast response function, we can rule out compressive nonlinearities,
161 because the functions accelerate at both the first and second harmonic frequencies. The explanation for this
162 difference could be due to different anatomical pathways. Binocular combination in the circadian system
163 likely takes place in the suprachiasmatic nucleus, whereas in the pupil constriction circuit the Edinger-
164 Westphal nucleus is the most likely site of binocular integration [9]. Presumably these anatomical differences,

165 and the practical constraints of the two systems, lead to differences in response.

166 Our recent psychophysical work [26] has looked at binocular interactions in the L-M and S-cone pathways, and
167 compared these to the light flux pathway. Using a contrast discrimination paradigm with spatial modulations
168 of light flux and colour, we found equally strong interocular suppression in all three pathways [26]. This
169 is rather different from our pupillometry results here, which demonstrate weaker suppression in the light
170 flux and S-cone pathways than in the L-M pathway (see Figure 2). However, the current experiments
171 involve temporal modulations, which are quite distinct from the spatial modulations used in our previous
172 work [26]. Our other recent work [3] has shown that temporal luminance modulations involve much weaker
173 interocular suppression in the cortical response than do spatial luminance modulations [27]. These different
174 normalization processes might reflect different priorities for spatial and temporal vision. Spatial vision aims
175 to fuse images to provide binocular single vision, and benefits from ‘ocularity invariance’ [20], in which
176 visual appearance is constant when viewed with one eye or two. Temporal vision is critical for motion
177 perception, which can involve alternative binocular computations, such as calculating velocity differences
178 between the eyes [28]. Of course the present measurements were of pupil size, which may be subject to
179 different anatomical and functional constraints from those in the cortex. Future research should aim to
180 extend our current findings to perception using psychophysical approaches.

181 6 Conclusions

182 We have demonstrated that binocular combination of temporal flickering light in the autonomic nervous
183 system depends on the photoreceptor pathway stimulated. We were able to elicit pupil responses by stimu-
184 lating the periphery of the retina and we were able to record contrast response functions for all photoreceptor
185 pathways. While all pathways showed non-linear combination, they varied in how the signals are combined,
186 particularly in the weight of interocular suppression. This was strong ($\omega \geq 1$) for L-M and melanopsin
187 signals at the first harmonic, and all pathways at the second harmonic. Suppression was weaker ($\omega < 1$) in
188 the light flux pathway (consistent with previous work), and also for S-cone directed modulations.

₁₈₉ **7 Materials and methods**

₁₉₀ **7.1 Participants**

₁₉₁ Twenty-four participants were recruited for each of the four experiments for a total of ninety-six adult
₁₉₂ participants (28 male, 68 female), whose ages ranged from 18 to 41. All participants had normal or corrected
₁₉₃ to normal vision, no known abnormalities of binocular or colour vision, and gave written informed consent.
₁₉₄ Our procedures were approved by the Ethics Committee of the Department of Psychology at the University
₁₉₅ of York (identification number 184).

₁₉₆ **7.2 Apparatus & stimuli**

₁₉₇ To present synchronised stimulus modulations independently to each eye, two light engines (Spec-
₁₉₈ traTuneLAB, which are thermally stable across time with active cooling according to the manufacturers:
₁₉₉ LEDMOTIVE Technologies, LLC, Barcelona, Spain), each with 10 independently addressable LED colour
₂₀₀ channels, were integrated into a customised binocular viewing system. The light engines were operated via
₂₀₁ a Python interface to their REST API [29], which supports synchronous launch and playback of spectral
₂₀₂ sequences prepared in advance and stored in JSON format. A special command was commissioned from
₂₀₃ LEDMOTIVE to allow two different stimulus files to be launched simultaneously from the two devices. The
₂₀₄ synchronisation of the spectra from the two devices was tested and showed that they were synchronised to
₂₀₅ within approximately 3ms.

₂₀₆ When preparing the spectral sequences, the age of participants was used to account for the yellowing of the
₂₀₇ lenses. We used the silent substitution technique [30] to selectively stimulate specific photoreceptor classes.
₂₀₈ Silent substitution exploits the fact that each photoreceptor class has a distinct spectral tuning that overlaps
₂₀₉ with the others. Using a multiprimary system, in which the primaries (i.e. LEDs) have different spectra, it
₂₁₀ is possible to target one class of photoreceptors while maintaining the others at a constant activity level,
₂₁₁ effectively silencing them [31,32]. We calculated silent substitution solutions using the *PySilSub* toolbox [33],
₂₁₂ using linear algebra. The outputs of the two light engines (see Figure 1b,c) were calibrated using an Ocean
₂₁₃ Optics Jaz spectroradiometer, which was wavelength-calibrated to an Argon lamp and intensity calibrated
₂₁₄ using a NIST-traceable light source. Each primary was also linearised using a polynomial fit (see Figure S1
₂₁₅ for details). We used the 10-degree cone fundamentals [34], and estimates of melanopsin absorbance spectra
₂₁₆ from CIE S 026 (discussed in a previous paper [33]) to calculate α -opic irradiance.

₂₁₇ The output from the light engines was directed through liquid light guides (LLG3-8H: Thorlabs Ltd, Cam-

218 bridgeshire, UK) and diffused onto semi-opaque and highly diffusive white glass discs with a diameter of 50
219 mm for even illumination (34-473: Edmund Optics, York, UK). The light guide gaskets were butt-coupled
220 to the light engine diffusers with threaded adapters (SM1A9, AD3LLG: Thorlabs Ltd, Cambridgeshire,
221 UK) and the exiting ends of the light guides were mated with 51 mm depth optical cylinders (SM2L20:
222 Thorlabs Ltd, Cambridgeshire, UK) via appropriately threaded adapters (AD3LLG, SM2A6: Thorlabs Ltd,
223 Cambridgeshire, UK). The stimulus diffuser discs were retained at the front end of the optical cylinders
224 approximately 51 mm from the light source, at which distance the output beam was sufficiently dispersed to
225 afford even illumination of the diffuser when viewed from the front. To guarantee safe illumination levels, a
226 circular neutral-density filter with the same diameter of the white glass discs (50 mm) and an optical density
227 of 0.6 log units was placed in the optical path between the light source and the diffusers. A small circular
228 piece of blackout material with a diameter of approximately 8 degrees (10 mm) was positioned centrally on
229 the front of each diffuser disc to aid as a fusion lock, as a fixation point, and to occlude the fovea.

230 The diffuser discs were positioned in the objective planes of the lenses of a modified VR headset (SHINECON
231 SC-G01, Dongguan Shinecon Industrial Co. Ltd., Guangdong, China), which was used by the participants to
232 view the stimuli. The stimuli were two discs of flickering light with a diameter of approximately 30 degrees,
233 which were fused together into a cyclopean percept resembling a donut-shaped ring of light, similar to that
234 used in other studies [5–7,35,36]. The VR headset modifications allowed for small adjustments to account
235 for individual differences in interpupillary distance and focal length. The use of this set up allowed us to
236 modulate the stimuli in three different ocular configurations, similar to the ones we used in our previous
237 study [3]: monocular, binocular and dichoptic. In the monocular configuration, the unstimulated eye still
238 saw a non-flickering disc of mean light flux. A schematic of the stimulation system is shown in Figure
239 1a. Pupillometry data were collected using a binocular Pupil Core eye-tracker headset (Pupil Labs GmbH,
240 Berlin, Germany [37]) running at 120 Hz, and the signals were recorded with the Pupil Capture software.

241 Our previous study [3] used a temporal frequency of 2Hz for foveal luminance flicker, and recorded EEG
242 data simultaneously with pupillometry. Initial pilot experiments indicated that this frequency was too high
243 to elicit measurable responses when stimulating individual photoreceptor pathways. For all experiments, we
244 therefore used a primary flicker frequency of 0.5Hz, as previous literature showed that this was slow enough
245 to elicit a pupil response from all photoreceptor classes [7]. We also focussed on only recording pupillometry
246 data as this frequency would be too slow to elicit steady-state EEG responses [38].

247 For all experiments, sinusoidal temporal modulations were presented against the same background spectrum
248 (matched between the eyes), which was used to achieve silent substitution in the three photoreceptor mod-
249 ulation experiments. The background spectra were defined by setting all channels to half maximum output

250 for the brighter of the two devices (STLab 1, left eye) and then using the STLab 1/STLab 2 calibration
251 ratio to find the equivalent settings for the companion device (STLab 2, right eye). The background spec-
252 trum illuminance was approximately 74 lux, or 68.5 cd/m^2 . The spectral power distributions and α -opic
253 irradiances of the background spectra for both eyes are shown in Figure 1c-d.

254 Silent substitution stimuli were prepared and calibrated for each participant with custom Python software [33]
255 and Python scripts. Estimates of photoreceptor spectral sensitivities for each participant were constructed
256 from the known photopigment absorbance spectra [34], taking account of the peak axial density of the
257 respective photopigments, as well as lens [34,39,40] and macular pigment density [40,41], in accordance with
258 the field size and age-dependant CIEPO06 observer model [42]. The melanopic and rhodopic action spectra
259 of the 32-year-old standard observer were taken from CIE S 026 [43] and then adjusted for age-related lens
260 transmittance with a spectral correction function, in line with the standard. Macular pigment correction
261 was not applied to the rhodopic and melanopic action spectra because rods are not present at the fovea and
262 ipRGCs sit above the retinal pigment layer [44].

263 In the light flux experiment, the stimulus intensity was increased and decreased relative to the background,
264 which we expected to modulate all photoreceptor classes (see Figure 1e,i). In the L-M cone modulation
265 experiment, we used silent substitution to increase the L-cone activity, and simultaneously decrease the
266 M-cone activity, during the first half-cycle of the sine wave. In the second half-cycle the polarity of the
267 modulation reversed (see Figure 1f,j). The maximum available L-M contrast was approximately 10%. In the
268 S-cone modulation experiment, we increased and decreased S-cone-directed signals, whilst keeping activity
269 in the other photoreceptors constant (see Figure 1g,k). Our system allowed a maximum contrast of 45%.
270 Finally, in the melanopsin experiment, we modulated the activity of the melanopsin-containing intrinsically
271 photoreceptive retinal ganglion cells, whilst keeping cone activity constant (see Figure 1h,l). The maximum
272 available melanopsin contrast was 22%. We assume that the activity of rods was constant at the high
273 background luminance intensity used here, and so did not attempt to silence rod activity in any condition, as
274 this would have greatly reduced the available dynamic range. Splatter on nominally silenced photoreceptors
275 was very small (see Figure 1j-l), well below the levels that would be expected to generate measurable pupil
276 modulations, although we can observe that the rods may not be saturated in the L-M and melanopsin-
277 directed stimuli (Figure 1j and 1l) and could intrude in these two experiments. We also estimated activation
278 of penumbral L and M cones [5,35,45], which was minimal (≤ 1.5 contrast; less than splatter on the open-field
279 cones) for melanopsin-directed stimuli. We note that the temporal frequency of our modulation (0.5Hz) is
280 well below the range where penumbral cone activation can elicit visible percepts, and that such percepts
281 fade after around 1 second [35], and do not typically affect pupil responses [7].

²⁸² **7.3 Procedure**

²⁸³ Before the start of each experiment, participants adjusted the objective planes of the lenses with the help
²⁸⁴ of the experimenter until the stimulus was in focus and they perceived the two pieces of blackout material
²⁸⁵ as one fused disc. Pupil responses to binocular temporal contrast modulations were examined in a factorial
²⁸⁶ design that combined six ocular conditions and five temporal contrast levels: 6, 12, 24, 48 and 96% of the
²⁸⁷ available dynamic range. This design, similar to that used in our previous studies [3,27,46], was applied
²⁸⁸ in four separate experiments, each with a different mode of photoreceptor stimulation. In the first three
²⁸⁹ conditions, the discs flickered at 0.5 Hz, in either a monocular, binocular or dichoptic arrangement. In the
²⁹⁰ dichoptic condition the non-target eye saw a flickering fixed contrast of 48% of the available dynamic range.
²⁹¹ In the remaining three conditions (the cross-frequency conditions) one eye's disc flickered at 0.4 Hz, and
²⁹² the other eye's disc flickered at 0.5 Hz. This included monocular responses at 0.4 Hz, as well as binocular
²⁹³ (one eye sees each frequency at the target contrast) and dichoptic (target stimulus flickering at 0.5 Hz, mask
²⁹⁴ contrast of 48% at 0.4 Hz in the other eye) arrangements. We counterbalanced presentation of the target
²⁹⁵ stimulus across the left and right eyes.

²⁹⁶ The experiments were conducted in a windowless room, in which the only source of light was the modified
²⁹⁷ VR headset. The participants sat as close as possible to the VR headset, leaving enough space for the
²⁹⁸ eye-tracker to record the eyes. Each experiment was carried out in a single session of around 45-60 minutes,
²⁹⁹ divided into three blocks of 15-17 minutes each. In each block, there were a total of 60 trials lasting 15
³⁰⁰ seconds each (12s of stimulus presentation, followed by 3s of interstimulus interval). The participants were
³⁰¹ given no task other than look at the black fixation dot while trying to minimise their blinking during the
³⁰² presentation period. For all experiments other than the light flux condition, participants adapted to the
³⁰³ unmodulated background luminance for two minutes before stimulation began.

³⁰⁴ Before the start of the L-M experiment, participants completed a luminance nulling perceptual calibration
³⁰⁵ procedure in L-M cone space on an Iiyama VisionMasterTM Pro 510 display (800 x 600 pixels, 60 Hz refresh
³⁰⁶ rate). During the task, participants were presented with a disc flickering within the L-M cone space (between
³⁰⁷ magenta and cyan). Using a trackball, participants adjusted the angle in cone space to find their subjective
³⁰⁸ isoluminant point, which resulted in changing the flickering intensity of the stimulus until the amplitude of
³⁰⁹ the flicker appeared to be minimised. The result was used to modify the requested contrasts during stimulus
³¹⁰ preparation so as to account for individual differences affecting perceived illuminance, principally the L:M
³¹¹ cone ratio [47,48].

312 **7.4 Data analysis**

313 The pupillometry data were analysed using the same method we used in our previous study [3]. The data
314 were converted from mp4 videos to a csv text file using the Pupil Player software [37], which estimated
315 pupil diameter for each eye on each frame using a 3D model of the eyeball. The individual data were then
316 loaded into R for analysis, where a ten-second waveform for each trial in each eye was extracted (excluding
317 the first two seconds after stimulus onset). We interpolated across any dropped or missing frames to ensure
318 regular and continuous sampling over time. The Fourier transform was calculated for each waveform, and all
319 repetitions of each condition were pooled across eye and then averaged. Finally, data were averaged across
320 all participants to obtain the group results. We used coherent averaging and at each stage we excluded data
321 points with a Mahalanobis distance exceeding $D = 3$ from the complex-valued mean [49]. For monocular
322 stimulation, we confirmed that the consensual response was equivalent to the response in the stimulated eye.
323 For all experiments, we used a bootstrapping procedure with 10^4 iterations to estimate standard errors across
324 participants. All analysis and figure construction was conducted using a single R-script, available online,
325 making this study fully computationally reproducible: <https://osf.io/gdvt4/>.

326 **7.5 Computational model and parameter estimation**

327 To quantitatively summarise our data, we used the same model described in our previous study [3]. The
328 model has the same general form as the first stage of the contrast gain control model proposed by Meese
329 and colleagues [22], but omits the second stage. For the previous model that we used [3], the exponent of
330 the numerator and denominator had fixed values of 2 and (implicitly) 1. Here, we allow these parameters
331 (called p and q) to be free, in order to permit different shapes of contrast response function, e.g. accelerating
332 or saturating. The responses of the left eye and right eye channels are as follows:

$$resp_L = \frac{L^p}{Z + L^q + \omega R^q}, \quad (1)$$

$$resp_R = \frac{R^p}{Z + R^q + \omega L^q}, \quad (2)$$

333 where L and R are the contrast signals from the left and right eyes, p and q are exponents, Z is a saturation
334 constant that shifts the contrast-response function laterally, and ω is the weight of suppression from the
335 other eye.

336 The responses from the two eyes are then summed binocularly:

$$resp_B = R_{max}(resp_L + resp_R) + k, \quad (3)$$

337 where k is a noise parameter, and R_{max} scales the overall response amplitude.

338 The models were fit using a hierarchical Bayesian framework implemented in Stan [50]. The data for each
339 photoreceptor type and response frequency was fit separately, for a total of 8 model fits. The prior for the ω
340 parameter was Gaussian, with a mean of 1 and standard deviation of 0.5. Priors for the other free parameters
341 were also Gaussian, with mean values based on previous work [3]. We calculated over 10^6 posterior samples,
342 and retained 10% for plotting.

343 8 References

- 344 1. McDougal DH, Gamlin PD. Autonomic control of the eye. *Comprehensive Physiology*. 2015;5: 439–473.
345 doi:[10.1002/cphy.c140014](https://doi.org/10.1002/cphy.c140014)
- 346 2. Wyatt HJ, Musselman JF. Pupillary light reflex in humans: Evidence for an unbalanced pathway from
347 nasal retina, and for signal cancellation in brainstem. *Vision Res.* 1981;21: 513–25. doi:[10.1016/0042-6989\(81\)90097-3](https://doi.org/10.1016/0042-6989(81)90097-3)
- 349 3. Segala FG, Bruno A, Martin JT, Aung MT, Wade AR, Baker DH. Different rules for binocular combination
350 of luminance flicker in cortical and subcortical pathways. *eLife*. 2023;12. doi:[10.7554/elife.87048](https://doi.org/10.7554/elife.87048)
- 351 4. McDougal DH, Gamlin PD. The influence of intrinsically-photosensitive retinal ganglion cells on the
352 spectral sensitivity and response dynamics of the human pupillary light reflex. *Vision Research*. 2010;50:
353 72–87. doi:[10.1016/j.visres.2009.10.012](https://doi.org/10.1016/j.visres.2009.10.012)
- 354 5. Barrionuevo PA, Cao D. Luminance and chromatic signals interact differently with melanopsin activation
355 to control the pupil light response. *Journal of Vision*. 2016;16(11): 29. doi:[10.1167/16.11.29](https://doi.org/10.1167/16.11.29)
- 356 6. Murray IJ, Kremers J, McKeeffry D, Parry NRA. Paradoxical pupil responses to isolated M-cone incre-
357 ments. *Journal of the Optical Society of America A*. 2018;35: B66–B71. doi:[10.1364/JOSAA.35.000B66](https://doi.org/10.1364/JOSAA.35.000B66)
- 358 7. Spitschan M, Jain S, Brainard DH, Aguirre GK. Opponent melanopsin and s-cone signals in the hu-
359 man pupillary light response. *Proceedings of the National Academy of Sciences*. 2014;111: 15568–15572.
360 doi:[10.1073/pnas.1400942111](https://doi.org/10.1073/pnas.1400942111)

- 361 8. Woelders T, Leenheers T, Gordijn MCM, Hut RA, Beersma DGM, Wams EJ. Melanopsin- and L-cone-
362 induced pupil constriction is inhibited by S- and M-cones in humans. *Proceedings of the National Academy*
363 *of Sciences*. 2018;115: 792–797. doi:[10.1073/pnas.1716281115](https://doi.org/10.1073/pnas.1716281115)
- 364 9. Mathôt S. Pupillometry: Psychology, physiology, and function. *J Cogn.* 2018;1: 16. doi:[10.5334/joc.18](https://doi.org/10.5334/joc.18)
- 365 10. Markwell EL, Feigl B, Zele AJ. Intrinsically photosensitive melanopsin retinal ganglion cell contributions
366 to the pupillary light reflex and circadian rhythm. *Clinical and Experimental Optometry*. 2010;93: 137–149.
367 doi:[10.1111/j.1444-0938.2010.00479.x](https://doi.org/10.1111/j.1444-0938.2010.00479.x)
- 368 11. Provencio I, Rodriguez IR, Jiang G, Hayes WP, Moreira EF, Rollag MD. A Novel Human Opsin in the
369 Inner Retina. *Journal of Neuroscience*. 2000;20: 600–605. doi:[10.1523/JNEUROSCI.20-02-00600.2000](https://doi.org/10.1523/JNEUROSCI.20-02-00600.2000)
- 370 12. Panda S, Sato TK, Castrucci AM, Rollag MD, DeGrip WJ, Hogenesch JB, et al. Melanopsin
371 (opn4) requirement for normal light-induced circadian phase shifting. *Science*. 2002;298: 2213–2216.
372 doi:[10.1126/science.1076848](https://doi.org/10.1126/science.1076848)
- 373 13. Ruby NF, Brennan TJ, Xie X, Cao V, Franken P, Heller HC, et al. Role of melanopsin in circadian
374 responses to light. *Science*. 2002;298: 2211–2213. doi:[10.1126/science.1076701](https://doi.org/10.1126/science.1076701)
- 375 14. Dacey DM, Peterson BB, Robinson FR, Gamlin PD. Fireworks in the primate retina: In
376 vitro photodynamics reveals diverse lgn-projecting ganglion cell types. *Neuron*. 2003;37: 15–27.
377 doi:[https://doi.org/10.1016/S0896-6273\(02\)01143-1](https://doi.org/10.1016/S0896-6273(02)01143-1)
- 378 15. Lucas RJ, Hattar S, Takao M, Berson DM, Foster RG, Yau K-W. Diminished pupillary light reflex at
379 high irradiances in melanopsin-knockout mice. *Science*. 2003;299: 245–247. doi:[10.1126/science.1077293](https://doi.org/10.1126/science.1077293)
- 380 16. Gamlin PDR, McDougal DH, Pokorny J, Smith VC, Yau K-W, Dacey DM. Human and macaque
381 pupil responses driven by melanopsin-containing retinal ganglion cells. *Vision Research*. 2007;47: 946–954.
382 doi:[10.1016/j.visres.2006.12.015](https://doi.org/10.1016/j.visres.2006.12.015)
- 383 17. Hubel DH, Wiesel TN. Receptive fields, binocular interaction and functional architecture in the cat's
384 visual cortex. *J Physiol.* 1962;160: 106–54. doi:[10.1113/jphysiol.1962.sp006837](https://doi.org/10.1113/jphysiol.1962.sp006837)
- 385 18. Baker DH, Lygo FA, Meese TS, Georgeson MA. Binocular summation revisited: Beyond $\sqrt{2}$. *Psychol*
386 *Bull.* 2018;144: 1186–1199. doi:[10.1037/bul0000163](https://doi.org/10.1037/bul0000163)
- 387 19. Campbell FW, Green DG. Monocular versus binocular visual acuity. *Nature*. 1965;208: 191–2.
388 doi:[10.1038/208191a0](https://doi.org/10.1038/208191a0)
- 389 20. Baker DH, Meese TS, Georgeson MA. Binocular interaction: Contrast matching and contrast discrimi-
390 nation are predicted by the same model. *Spat Vis.* 2007;20: 397–413. doi:[10.1163/156856807781503622](https://doi.org/10.1163/156856807781503622)

- 391 21. Moradi F, Heeger DJ. Inter-ocular contrast normalization in human visual cortex. *J Vis.* 2009;9: 13.1–22.
392 doi:[10.1167/9.3.13](https://doi.org/10.1167/9.3.13)
- 393 22. Meese TS, Georgeson MA, Baker DH. Binocular contrast vision at and above threshold. *Journal of*
394 *Vision.* 2006;6: 1224–43. doi:[10.1167/6.11.7](https://doi.org/10.1167/6.11.7)
- 395 23. Kingdom FAA, Libenson L. Dichoptic color saturation mixture: Binocular luminance contrast promotes
396 perceptual averaging. *J Vis.* 2015;15: 2. doi:[10.1167/15.5.2](https://doi.org/10.1167/15.5.2)
- 397 24. Busse L, Wade AR, Carandini M. Representation of concurrent stimuli by population activity in visual
398 cortex. *Neuron.* 2009;64: 931–42. doi:[10.1016/j.neuron.2009.11.004](https://doi.org/10.1016/j.neuron.2009.11.004)
- 399 25. Spitschan M, Cajochen C. Binocular facilitation in light-mediated melatonin suppression? *J Pineal Res.*
400 2019;67: e12602. doi:[10.1111/jpi.12602](https://doi.org/10.1111/jpi.12602)
- 401 26. Baker DH, Hansford KJ, Segala FG, Morsi AY, Huxley RJ, Martin JT, et al. Binocular integration of
402 chromatic and luminance signals. *J Vis.* 2024;24(12): 7. doi:[10.1167/jov.24.12.7](https://doi.org/10.1167/jov.24.12.7)
- 403 27. Baker DH, Wade AR. Evidence for an optimal algorithm underlying signal combination in human visual
404 cortex. *Cereb Cortex.* 2017;27: 254–264. doi:[10.1093/cercor/bhw395](https://doi.org/10.1093/cercor/bhw395)
- 405 28. Kaestner M, Maloney RT, Wailes-Newson KH, Bloj M, Harris JM, Morland AB, et al. Asymmetries
406 between achromatic and chromatic extraction of 3D motion signals. *Proc Natl Acad Sci U S A.* 2019;116:
407 13631–13640. doi:[10.1073/pnas.1817202116](https://doi.org/10.1073/pnas.1817202116)
- 408 29. Martin JT, Pinto J, Bulte D, Spitschan M. PyPlr: A versatile, integrated system of hardware and
409 software for researching the human pupillary light reflex. *Behavior Research Methods.* 2022;54: 2720–2739.
410 doi:[10.3758/s13428-021-01759-3](https://doi.org/10.3758/s13428-021-01759-3)
- 411 30. Estévez O, Spekreijse H. The "silent substitution" method in visual research. *Vision Research.* 1982;22:
412 681–691. doi:[10.1016/0042-6989\(82\)90104-3](https://doi.org/10.1016/0042-6989(82)90104-3)
- 413 31. Shapiro AG, Pokorny J, Smith VC. Conerod receptor spaces with illustrations that use CRT phos-
414 phor and light-emitting-diode spectra. *Journal of the Optical Society of America A.* 1996;13: 2319.
415 doi:[10.1364/josaa.13.002319](https://doi.org/10.1364/josaa.13.002319)
- 416 32. Spitschan M, Woelders T. The Method of Silent Substitution for Examining Melanopsin Contributions
417 to Pupil Control. *Frontiers in Neurology.* 2018;9. doi:[10.3389/fneur.2018.00941](https://doi.org/10.3389/fneur.2018.00941)
- 418 33. Martin JT, Boynton GM, Baker DH, Wade AR, Spitschan M. PySilSub: An open-source python toolbox
419 for implementing the method of silent substitution in vision and nonvisual photoreception research. *Journal*
420 *of Vision.* 2023;23: 10. doi:[10.1167/jov.23.7.10](https://doi.org/10.1167/jov.23.7.10)

- 421 34. Stockman A, Sharpe LT. The spectral sensitivities of the middle- and long-wavelength-sensitive cones de-
422 rived from measurements in observers of known genotype. *Vision Res.* 2000;40: 1711–37. doi:[10.1016/s0042-6989\(00\)00021-3](https://doi.org/10.1016/s0042-6989(00)00021-3)
- 424 35. Spitschan M, Aguirre GK, Brainard DH. Selective stimulation of penumbral cones reveals perception in
425 the shadow of retinal blood vessels. *PLoS One.* 2015;10: e0124328. doi:[10.1371/journal.pone.0124328](https://doi.org/10.1371/journal.pone.0124328)
- 426 36. Zele AJ, Feigl B, Adhikari P, Maynard ML, Cao D. Melanopsin photoreception contributes to human
427 visual detection, temporal and colour processing. *Scientific Reports.* 2018;8. doi:[10.1038/s41598-018-22197-w](https://doi.org/10.1038/s41598-018-22197-w)
- 429 37. Kassner M, Patera W, Bulling A. Pupil: An open source platform for pervasive eye tracking and
430 mobile gaze-based interaction. *Proceedings of the 2014 ACM international joint conference on pervasive and
431 ubiquitous computing: Adjunct publication.* ACM; 2014. doi:[10.1145/2638728.2641695](https://doi.org/10.1145/2638728.2641695)
- 432 38. Norcia AM, Appelbaum LG, Ales JM, Cottreau BR, Rossion B. The steady-state visual evoked potential
433 in vision research: A review. *Journal of Vision.* 2015;15(6): 4. doi:[10.1167/15.6.4](https://doi.org/10.1167/15.6.4)
- 434 39. Pokorny J, Smith VC, Lutze M. Aging of the human lens. *Applied Optics.* 1987;26: 1437.
435 doi:[10.1364/ao.26.001437](https://doi.org/10.1364/ao.26.001437)
- 436 40. Stockman A, Sharpe LT, Fach C. The spectral sensitivity of the human short-wavelength sen-
437 sitive cones derived from thresholds and color matches. *Vision Research.* 1999;39: 2901–2927.
438 doi:[https://doi.org/10.1016/S0042-6989\(98\)00225-9](https://doi.org/10.1016/S0042-6989(98)00225-9)
- 439 41. Bone RA, Landrum JT, Fernandez L, Tarsis SL. Analysis of the macular pigment by HPLC: Retinal
440 distribution and age study. *Investigative Ophthalmology & Visual Science.* 1988;29: 843–849.
- 441 42. CIE. Fundamental chromaticity diagram with physiological axes. CIE Central Bureau; 2006. Available:
442 <https://cie.co.at/publications/fundamental-chromaticity-diagram-physiological-axes-part-1>
- 443 43. CIE. CIE system for metrology of optical radiation for ipRGC-influenced responses to light. CIE Central
444 Bureau; 2018. doi:[10.25039/S026.2018](https://doi.org/10.25039/S026.2018)
- 445 44. Trieschmann M, Kuijk FJGM van, Alexander R, Hermans P, Luthert P, Bird AC, et al. Macular
446 pigment in the human retina: Histological evaluation of localization and distribution. *Eye.* 2007;22: 132–
447 137. doi:[10.1038/sj.eye.6702780](https://doi.org/10.1038/sj.eye.6702780)
- 448 45. Zele AJ, Adhikari P, Cao D, Feigl B. Melanopsin driven enhancement of cone-mediated visual processing.
449 *Vision Res.* 2019;160: 72–81. doi:[10.1016/j.visres.2019.04.009](https://doi.org/10.1016/j.visres.2019.04.009)

- 450 46. Baker DH, Vilidaite G, McClarnon E, Valkova E, Bruno A, Millman RE. Binaural summation of
451 amplitude modulation involves weak interaural suppression. *Sci Rep.* 2020;10: 3560. doi:[10.1038/s41598-020-60602-5](https://doi.org/10.1038/s41598-020-60602-5)
- 453 47. Carroll J, Neitz J, Neitz M. Estimates of L:M cone ratio from ERG flicker photometry and genetics.
454 *Journal of Vision.* 2002;2: 1. doi:[10.1167/2.8.1](https://doi.org/10.1167/2.8.1)
- 455 48. Hofer H, Carroll J, Neitz J, Neitz M, Williams DR. Organization of the human trichromatic cone mosaic.
456 *The Journal of Neuroscience.* 2005;25: 9669–9679. doi:[10.1523/jneurosci.2414-05.2005](https://doi.org/10.1523/jneurosci.2414-05.2005)
- 457 49. Baker DH. Statistical analysis of periodic data in neuroscience. *Neurons, Behavior, Data analysis, and*
458 *Theory.* 2021;5. doi:[10.51628/001c.27680](https://doi.org/10.51628/001c.27680)
- 459 50. Carpenter B, Gelman A, Hoffman MD, Lee D, Goodrich B, Betancourt M, et al. Stan: A probabilistic
460 programming language. *J Stat Softw.* 2017;76. doi:[10.18637/jss.v076.i01](https://doi.org/10.18637/jss.v076.i01)

9 Supplementary material

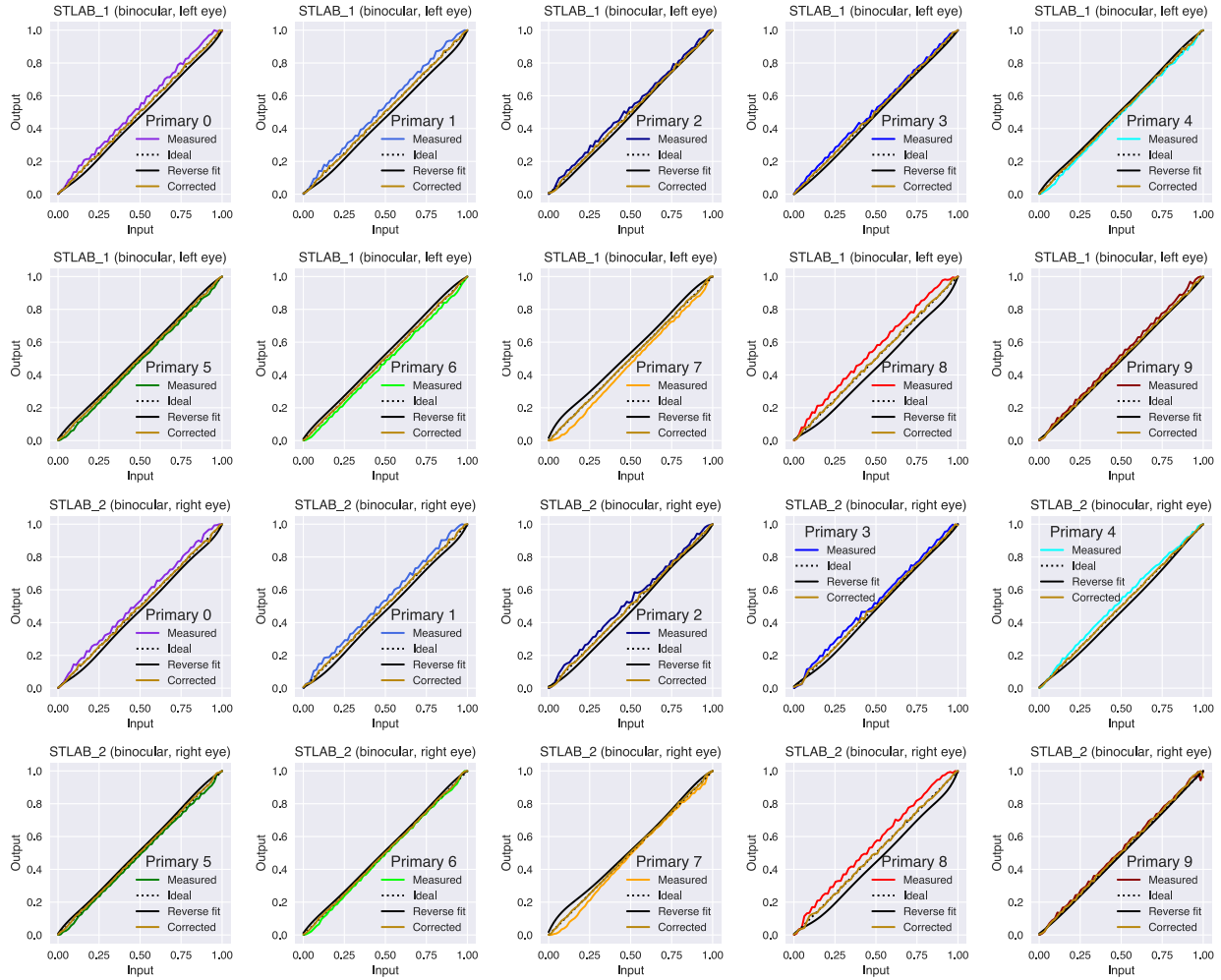


Figure S1: Linearity of primaries for each device. The calibration measures were summed (i.e., total unweighted irradiance), and the input-output relationship summarised by a 7th order polynomial reverse curve fit. By applying the coefficients of the regression, it is possible to achieve a linear output in the primaries.